Chemical Engineering Science 189 (2018) 65–74

Contents lists available at ScienceDirect

Chemical Engineering Science

journal homepage: www.elsevier.com/locate/ces

CO_2 adsorption performance of functionalized metal-organic frameworks of varying topologies by molecular simulations

Wei Li, Song Li *

State Key Laboratory of Coal Combustion, School of Energy and Power Engineering, Huazhong University of Science and Technology, 430074, China
Shenzhen Research Institute of Huazhong University of Science and Technology, Shenzhen 518057, China
Nano Interface Centre for Energy, School of Energy and Power Engineering, Huazhong University of Science and Technology, 430074, China

HIGHLIGHTS

- Pore sizes play a dominating role in CO_2 capture.
- Pore size-dependent CO_2 adsorption was only observed for MOFs in *ftw*, but not for MOFs in *csq* and *scu*.
- The enhancement in CO_2 adsorption of MOFs upon functionalization also depends on pore sizes.

GRAPHICAL ABSTRACT

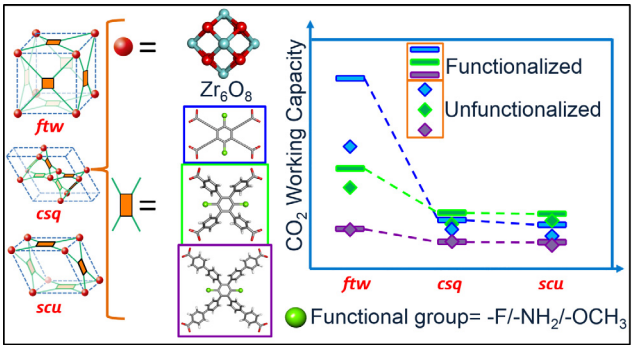

ARTICLE INFO

Article history:
Received 7 December 2017
Received in revised form 27 March 2018
Accepted 23 May 2018
Available online 24 May 2018

Keywords:
Carbon capture
Adsorption
Topology
Pore size
Functionalization

ABSTRACT

The mixed linker metal-organic frameworks (MOFs) consisting of a variety of organic linkers functionalized by multiple functional groups exhibit better performance in carbon capture due to the increased surface heterogeneity. In order to explore the influence of the framework topology and mixed functionalities on the carbon capture performance, in this work, Zr-MOFs in three topologies (*csq*, *ftw*, *scu*) with each composed by one of the three types of linkers of different lengths were constructed, which were then functionalized by three types of functional groups (—F, —NH_2, —OCH_3), respectively. Grand canonical Monte Carlo (GCMC) simulations were used to investigate CO_2 adsorption performance of all created MOFs. We revealed that among the parent MOFs consisted of identical building blocks but in different topologies, *ftw*-MOFs exhibit the highest CO_2 working capacity and CO_2/N_2 selectivity due to the strong affinity towards CO_2. Moreover, the CO_2 adsorption performance of *ftw*-MOFs shows obvious dependence on the pore size, consistent with their host-adsorbate interaction energy, which is not the fact for *csq*-MOFs and *scu*-MOFs. The enhanced CO_2 adsorption performance upon functionalization of MOFs displays pore-size dependence as well, especially for —NH_2 functionalized frameworks in *csq* and *scu*, which is mostly attributed to the enhanced host-adsorbate Coulombic interaction. The proposed effects of the topology, the pore size and the functional group on CO_2 adsorption performance of MOFs obtained in this study may provide meaningful insight into the rational design of high-performing MOFs for carbon capture by tuning the topology, pore size and functionality of frameworks.

© 2018 Elsevier Ltd. All rights reserved.

1. Introduction

Anthropogenic carbon dioxide (CO_2) is the major greenhouse gas in the atmosphere that leads to global climate change. The

* Corresponding author at: State Key Laboratory of Coal Combustion, School of Energy and Power Engineering, Huazhong University of Science and Technology, 430074, China.
E-mail address: songli@hust.edu.cn (S. Li).

https://doi.org/10.1016/j.ces.2018.05.042
0009-2509/© 2018 Elsevier Ltd. All rights reserved.

CO_2 emissions related to human activities result primarily from the combustion of fossil fuels and various chemical processes. Renewable energy (such as hydroenergy and biomass energy) is still far from replacing fossil fuels as the primary energy. Therefore, carbon capture and sequestration (CCS) plays an important role in facing this challenge as well as providing viable technologies that can deal with the emission from fossil fuels.

Currently, a variety of strategies including membrane separation, chemical absorption, physical adsorption, cryogenic separation, electrochemical separation, and fuel cells, have been proposed to sequester CO_2 from the combustion of fossil fuels. In particular, among several separation strategies, adsorption based-on metal-organic frameworks (MOFs) is regarded as a promising means to efficiently capture CO_2 (Sumida et al., 2012). MOFs are a class of nanoporous materials containing periodic networks of metals, metal clusters, or metal oxide clusters held together by bridging organic linkers (Furukawa et al., 2013). Compared with other traditional adsorbents used in industry, such as zeolites, activated carbon and silica, MOFs possess a variety of outstanding features, including ultra-high surface area, well-defined pore properties, especially the tunable and tailorable structures and chemical functionalities (Li et al., 2012). The ultrahigh surface area and tunable pore surface chemistry endow MOFs with higher adsorption capacity and selectivity toward CO_2 than activated carbons and zeolites (D'Alessandro et al., 2010). As a new type of functional adsorbent materials, MOFs have undergone extensive development and rapid progress in carbon capture over the past several decades (Liu et al., 2012; Long and Yaghi, 2009). Britt et al. reported that Mg-MOF-74 with exposed magnesium exhibited the CO_2 adsorption capacity up to 8.48 mmol/g at 0.1 MPa, and undergone facile CO_2 release at significantly lower temperature, 80 °C (Britt et al., 2009). However, design of MOFs with exceptionally high capacity and selectivity toward CO_2 adsorption remains challenging, since most of the MOFs adsorb not only CO_2 but also a considerable amount of other impurities, such as N_2, and CH_4 (Liu et al., 2012). Therefore, it is of great importance to tailor the pore metrics and functionality of MOFs specifically for CO_2 capture (Banerjee et al., 2009; Eddaoudi et al., 2002).

Both prefunctionalization of organic linkers and postsynthetic modification of pore surface are frequently used strategies for improving the gas adsorption performance (Devic et al., 2010; Evans et al., 2014; Tanabe and Cohen, 2011). Yaghi's group firstly reported functionalized isoreticular metal-organic frameworks (IRMOFs) by various functional groups including —Br and —NH_2 for methane storage (Eddaoudi et al., 2002), and they synthesized a series of zeolitic imidazolate frameworks (ZIFs) modified by polar or nonpolar functional groups, among which ZIF-78 functionalized by —NO_2 polar groups exhibited the highest CO_2 uptake and selectivity due to the strong dipole-quadrupole interaction between polar functional groups and CO_2 molecules (Banerjee et al., 2009). Couck et al. (2009) found that the CO_2/CH_4 selectivity of amine-functionalized MIL-53(Al) was increased by several orders of magnitude without compensating the CO_2 adsorption capacity due to the enhanced affinity towards CO_2 after introducing —NH_2. Reinsch et al. integrated various functional groups into the aromatic rings of CAU-10, respectively and revealed the order of CO_2 adsorption capability of modified CAU-10: —NO_2 > —NH_2 > —CH_3 > —OH > —OCH_3 (Reinsch et al., 2013). Jiang et al. (2012) prepared a series of functionalized PCN-58 and found that amine-anchored PCN-58 shown the highest selectivity toward CO_2 over N_2 among diversely functionalized frameworks. Then, McDonald et al. (2015) reported the highly efficient CO_2 capture performance of diamine-appended M_2(dobpdc) based on the cooperative process of CO_2 insertion and the formation of well-ordered ammonium carbamate by pore surface amines. Computational modelling revealed similar findings that the introduction of functional groups with stronger electron-donating abilities into frameworks may lead to high adsorption selectivity towards CO_2 (Liu and Zhong, 2010).

All the above-mentioned MOFs are composed of the same type of linkers carrying identical functional groups within one framework (mono-linker MOFs). Recently, introducing multiple differently functionalized linkers into one framework (*i.e.* multivariate MOFs, MTV-MOFs) to promote the pore surface heterogeneity for better adsorption performance was proposed and implemented. In 2010, Deng et al. (2010) reported the ultrahigh CO_2 selectivity of the derived MOF-5 by integrating various functionalities into the frameworks, which was attributed to the synergistic effects of varying functional groups according to the study of McDaniel et al. (2013) They later proved that the spatial apportionment of functional groups within frameworks imposed great effects on the adsorption performance of MTV-MOFs by the combined investigations of solid-state nuclear magnetic resonance and molecular simulations (Kong et al., 2013). Nevertheless, the preparation of MTV-MOFs with precisely positioned functional groups is exceedingly challenging due to the competition between different kinetically and thermodynamically favored products. Recently, Yuan et al. developed a kinetically controlled synthetic strategy, *i.e.* sequential linker installation to realize the precisely control of multiple functional groups within one framework (Yuan et al., 2015). They successfully synthesized a series of Zr-based PCN-700 consisting of different-length linkers with a variety of functional groups, whose H_2 adsorption capacity were increased by 57% in contrast to their parent counterparts (Yuan et al., 2016). The success of sequential linker installation strategy in PCN-700 paves the way for experimentally obtaining an enormous number of MTV-MOFs with enhanced structural and functional diversity by integrating multiple functionalities to engineer the pore environment.

On the other hand, *in silico* design and computational screening of high-performance MTV-MOFs were also conducted. McDaniel et al. (2013) ascribed the enhancement in gas uptake of mixed linker MOF-5 to the cooperative adsorbate-linker interaction involving multiple functionalities by molecular simulations. Collins et al. (2016) have optimized the CO_2 capacity of experimentally characterized MOFs by evolving the functional groups within the pores using the genetic algorithm, and demonstrated the importance of multiple functionalities in improving CO_2 uptake. Recently, we performed a high-throughput computational screening of $\sim 1 \times 10^4$ computer-generated MTV-MOFs in *pcu* topology to evaluate their CO_2 capture performance by grand canonical Monte Carlo (GCMC) simulations. The results demonstrated that the enhanced CO_2 adsorption performance of MTV-MOFs compared with their unfunctionalized counterparts was mainly attributed to the pore size instead of the presence of the three functionalities (—F, —NH_2 and —OCH_3). MTV-MOFs with small pore sizes generally gave rise to high CO_2 uptake and CO_2/N_2 selectivity compared with the ones with big pore sizes irrespective of their multiple functionalities (Li et al., 2017). Nevertheless, it is still unknown whether the dominant role of pore size in carbon capture performance of *pcu*-MTV-MOFs are applicable to the MOFs in different topologies. In order to explore the effects of functionalization, pore sizes and topologies on carbon capture performance of MOFs, in this work we performed a systematic study on Zr-based MOFs of *csq*, *ftw* and *scu* topologies by grand canonical Monte Carlo (GCMC) simulations. The linkers of different lengths, and multiple functionalities including —F, —NH_2 and —OCH_3 were introduced into the frameworks in order to study their impacts on the carbon capture performance.

2. Methodology

2.1. MOFs construction

Zr-based MOFs, which exhibit rich structure diversity, outstanding stability and intriguing functionalities, are promising MOFs for practical applications (Bai et al., 2016). In this work, to assess the carbon capture performance of MOFs judiciously, all the MOFs were generated with identical Zr-based metal node and organic linkers. In details, all the MOF structures were derived from Zr-based mono-linker MOFs in *csq*, *ftw* or *scu* topologies consisting of linkers in different lengths: 3,3′,3″,3‴-(benzene-1,2,4,5-tetrayl)tetrapropiolic acid (P4T), 4′,5′-bis(4-carboxyphenyl)-[1,1′:2′,1″-terphenyl]-4,4″-dicarboxylic acid (P4P) and 4″,5″-bis(4′-carboxy-[1,1′-biphenyl]-4-yl)-[1,1′:4′,1″:2″,1‴:4‴,1⁗-quinquephenyl]-4,4⁗-dicarboxylic acid (P4PP) (Fig. 1). In total, nine parent mono-linker MOFs were created as shown in Table 1. Three types of functional groups including —F (denoted as functional group "A"), —NH_2 (denoted as functional group "B") and —OCH_3 (denoted as functional group "C") were employed to functionalize the above nine parent MOFs. They were chosen as representatives of functionalities exhibiting different geometrical shapes and affinities towards CO_2 adsorbates. Each linker was functionalized at the opposing —H sites of the central aromatic ring in the linker by two identical functional groups. Given that each unit cell of *csq*-MOFs and *ftw*-MOFs have six linkers, each unit cell of *scu*-MOFs have four linkers, there are three types of functional groups coexisting in functionalized *csq*-MOFs and *ftw*-MOFs, but only two types coexisting in functionalized *scu*-MOFs. Due to the spatial symmetry of MOF structures, ten *csq*-MOF, ten *ftw*-MOF and six *scu*-MOF derivatives were constructed eventually, which have not been reported previously. The derived MOFs were named according to the combination type of functional groups, *e.g.* ABC denotes the framework simultaneously functionalized by three types of functional groups: A, B and C.

Geometry optimization of all the MOFs were implemented in the Forcite module of Materials Studio (Segall), which has been demonstrated to be a reliable tool in previous studies (Farha et al., 2010; Sim et al., 2014). The largest cavity diameter (LCD) was calculated using Zeo++ (Willems et al., 2012). The accessible surface area of frameworks was obtained from RASPA (Dubbeldam et al., 2014) with a nitrogen probe radius of 1.86 Å.

Table 1
The largest cavity diameter (LCD) and total surface area of parent MOFs in *csq*, *ftw* and *scu* topology calculated from Zeo++ (Willems et al., 2012) and RASPA (Dubbeldam et al., 2014), respectively.

Topology	Organic linker	LCD (Å)	Total surface area (m^2/g)
csq	P-4T	23.90	1887
	P-4P	28.97	2279
	P-4PP	41.76	4181
ftw	P-4T	10.01	1601
	P-4P	11.31	1908
	P-4PP	15.92	4235
scu	P-4T	9.00	1941
	P-4P	11.32	2315
	P-4PP	17.51	4262

2.2. Force field

The Lennard-Jones and Coulomb potentials were used to describe the non-bonded interaction between MOFs and adsorbates.

$$V_{ij} = 4\varepsilon_{ij}\left[\left(\frac{\sigma_{ij}}{r_{ij}}\right)^{1/2} - \left(\frac{\sigma_{ij}}{r_{ij}}\right)\right] + \frac{q_i q_j}{4\pi\varepsilon_0 r i_j} \quad (2\text{-}1)$$

Herein, *ij* represents the two interacting particles; ε is the depth of the potential wall; σ_{ij} is the finite distance at which the inter-particle potential is zero; r_{ij} is the distance between the particles. The q_i and q_j are the atomic partial charges of two interacting atoms, and ε_0 is the vacuum permittivity constant. All the LJ parameters of MOFs were taken from UFF force field (Rappe et al., 1992). The LJ parameters for N_2 and CO_2 were adapted from TraPPE force field (Potoff and Siepmann, 2001). The Lorentz-Berthelot mixing rule was applied for inter-atomic LJ interactions. Long-range Coulombic interaction was described by Ewald method (Essmann et al., 1995) with a cutoff of 12.8 Å.

The partial charges of all the MOFs were computed using the DDEC6 method (Manz and Limas, 2016), in which the atomic partial charges were obtained by fitting the electrostatic surface potential from plan-wave density functional theory (DFT) calculation using the Vienna ab initio simulation package (VASP) package (Hafner, 2008). The density derived electrostatic and chemical (DDEC) (Manz and Limas, 2016) method partitions the electron and spin densities to compute net atomic charges. The electron–ion interaction was described by the projector scheme with an

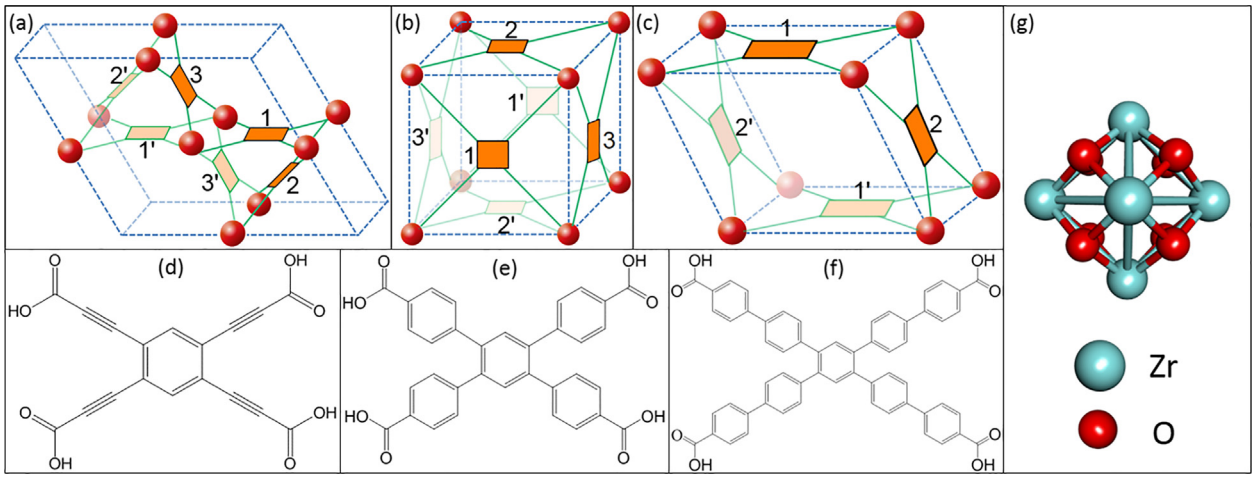

Fig. 1. Zr-based MOFs in (a) *csq*, (b) *ftw* and (c) *scu* topology. 1 and 1′, 2 and 2′, and 3 and 3′ represent equivalent linkers that will be simultaneously functionalized by identical functional groups (*i.e.* —F (A), —NH_2 (B) or —OCH_3 (C)). For example, the combination type "ABC" indicates that linkers 1 and 1' were functionalized by A, linkers 2 and 2' were functionalized by B, and linkers 3 and 3' were functionalized by C. All functionalization sites were located in the central benzene ring of the linkers (d) P4T, (e) P4P and (f) P4PP. The Zr-based inorganic node was presented in (g).

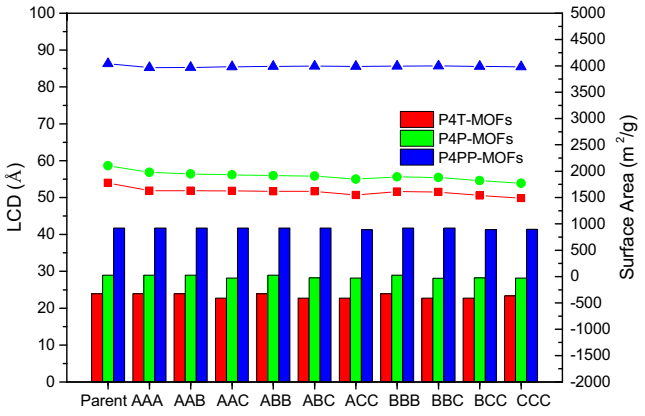

Fig. 2. The LCD and total surface area of *csq*-MOFs. The columns denote the LCDs of frameworks and the lined symbols are total surface areas of MOFs. The red, green and blue symbols represent P4T-MOFs, P4P-MOFs and P4PP-MOFs, respectively. (For interpretation of the references to colour in this figure legend, the reader is referred to the web version of this article.)

energy cutoff of 450 eV. A 1 × 1 × 1 Monkhorst-Pack k-point mesh was used for Brillouin zone sampling in the reciprocal space with spin polarization.

2.3. Grand canonical Monte Carlo simulations

All the GCMC simulations were carried out using the version 1.9 of RASPA simulation code (Dubbeldam et al., 2014). The total 1 × 10^6 Monte Carlo cycles were performed to obtain the adsorption properties of MOFs. After the initial 5 × 10^5 cycles of equilibration run, the additional 5 × 10^5 cycles were conducted for production run. Monte Carlo moves of insertion, deletion, rotation and translation were implemented with equal probability. Identity change for CO_2/N_2 mixture was performed with two times of the probability of insertion, deletion, rotation and translation moves. The simulation temperature was maintained at 298 K with the adsorption pressure ranging from 0.1 bar to 1 bar, similar to the reported adsorption/desorption pressures by vacuum swing adsorption (VSA) (Bae and Snurr, 2011; Sekizkardes et al., 2014). The molar ratio of CO_2/N_2 mixture was 1:9. CO_2 working capacity and CO_2/

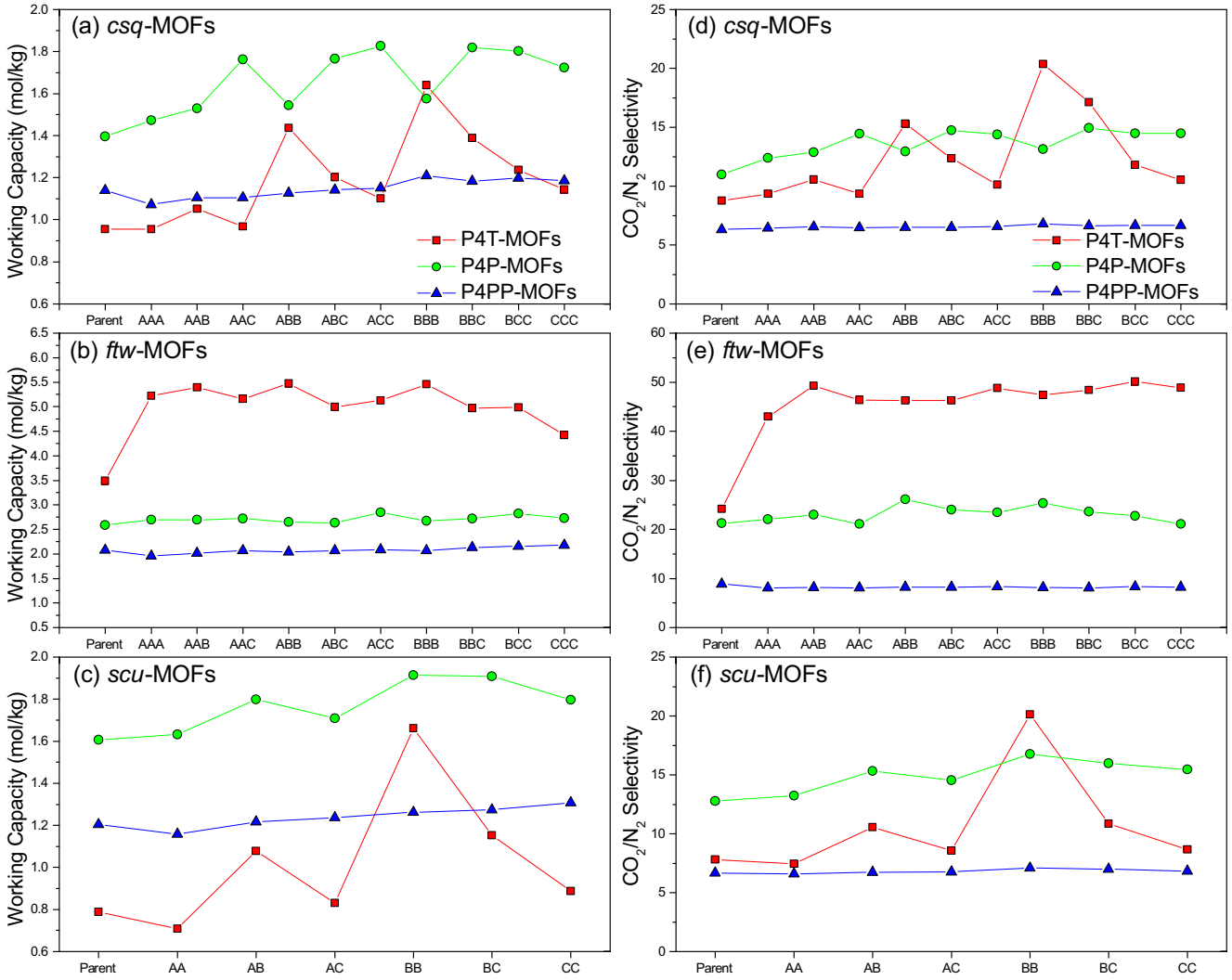

Fig. 3. The CO_2 working capacity (a, b, c) and CO_2/N_2 selectivity (d, e, f) of *csq*-, *ftw*- and *scu*-MOFs. The red, green and blue lines represent P4T-MOFs, P4P-MOFs and P4PP-MOFs, respectively. CO_2/N_2 selectivity was calculated at 298 K and 1 bar with the molar ratio of CO_2:N_2 = 1:9. (For interpretation of the references to colour in this figure legend, the reader is referred to the web version of this article.)

N_2 selectivity from GCMC simulations was computed using the following equations:

$$Working\,Capacity = Q_{CO_2,1bar} - Q_{CO_2,0.1bar} \quad (2\text{-}2)$$

$$Selectivity = \frac{Q_{CO_2}/Q_{N_2}}{f_{CO_2}/f_{N_2}} \quad (2\text{-}3)$$

Q_i, the uptake of gas component i; f_i, the fraction of gas component i in the mixture.

To compute the free energy contours of CO_2 molecule, three-dimensional grid points were superimposed on the unit cell of the structure with a grid spacing of 0.05 Å. The Edwald precision is 1×10^{-6}. The rotation number for CO_2 molecules is 1×10^5. At each point, the excess free energy of a CO_2 molecule with the center of mass (*i.e.* the C atom) positioned at that point was computed. The entropic contribution to the free energy comes from the rotational degrees of freedom of a CO_2 molecule. The detailed method has been described in our previous study (Li et al., 2017). The free energy distribution of each MOF was obtained by integratig the free energy of each grid within a framework.

3. Results and discussion

3.1. Structural properties

Among the MOFs consisting of identical building blocks, *csq*-MOFs exhibit the largest cavity diameter (LCD) followed by *ftw*- and *scu*-MOFs (Table 1). Regarding their surface area, *scu*-MOFs have the highest surface area in contrast to *csq*- and *ftw*- counterparts. In most cases, placing functional groups in MOF frameworks leads to decreased pore size (Banerjee et al., 2009; Eddaoudi et al., 2002). In this work, however, both the LCD and surface area of functionalized MOFs were not significantly changed compared with their parent counterparts as shown in *csq*-MOFs of Fig. 2. Similar tendency was also observed in *ftw*- and *scu*-MOFs of Figs. S1 and S2 in Supporting Information (SI), which can be mainly attributed to the large pore size of MOFs used in this work. The small volume ratios of introduced functional groups relative to the void volume of frameworks did not result in remarkable difference in the pore sizes and surface areas of MOFs derived from identical parents.

3.2. Carbon capture performance

Interestingly, the CO_2 working capacity and CO_2/N_2 selectivity of the functionalized MOFs and their parent counterparts exhibit dependence on the topology (Fig. 3). In general, among *csq*-, *ftw*- and *scu*-MOFs, *ftw*-P4T-MOFs show the highest CO_2 working capacity and CO_2/N_2 selectivity followed by medium-sized *ftw*-P4P-MOFs and large-sized *ftw*-P4PP-MOFs, which agrees with previous reports that the smaller the pore size is, the higher the CO_2 uptake and CO_2/N_2 selectivity are (Li et al. (2017). The density distribution maps of CO_2 molecules in parent MOFs of Fig. 4 demonstrate that the densities of CO_2 adsorbates in *ftw*-MOFs exhibit pore-size dependence as well. A vast majority of CO_2 molecules is accumulated in the small pores or located near the metal clusters of frameworks. With the linker length increases from P4T to P4PP, the clusters formed by adsorbed CO_2 molecules in small pores of P4T-MOFs nearly disappear in P4PP-MOFs, in accordance with the CO_2 working capacity observed in *ftw*-MOFs.

Nevertheless, the pore-size dependence of CO_2 working capacity and CO_2/N_2 selectivity is not applicable to *csq*-MOFs and *scu*-MOFs. In general, *csq*-P4P-MOFs with medium pore sizes exhibit higher CO_2 working capacity and selectivity than small *csq*-P4T-MOFs and large *csq*-P4PP-MOFs, similar to the trend observed in *scu*-MOFs. The unusual trend in *csq*- and *scu*-MOFs suggests the reliance of CO_2 adsorption performance on the topologies of frameworks.

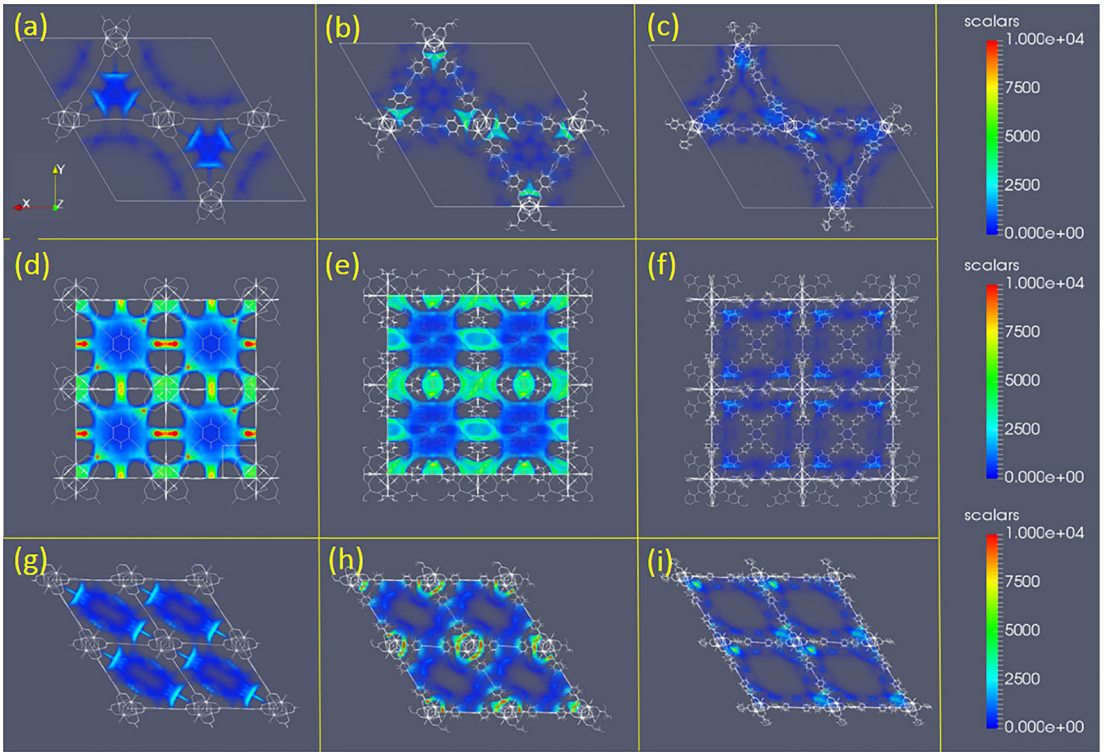

Fig. 4. The density distribution maps of CO_2 adsorbates in *csq*- (a, b, c), *ftw*- (d, e, f) and *scu*-MOFs (g, h, i) consisting of P4T (a, d, g), P4P (b, e, h) and P4PP (c, f, i) linkers at 298 K and 1 bar.

In order to further explore the mechanism underlying such a phenomenon, we computed the heat of desorption (Q_{st}) of CO_2 molecules as shown in Fig. 5, in which the overall variation in Q_{st} agreed well with the changes in CO_2/N_2 selectivity including *csq*- and *scu*-MOFs, but did not match the changes in CO_2 working capacity of *csq*- and *scu*-MOFs of Fig. 3. Given that CO_2 working capacity of Fig. 3 is expressed as the number of moles per unit weight of MOFs, in order to directly correlate the adsorption capacity with the geometrical properties of MOFs, we further converted the unit of CO_2 working capacity into the number of moles per unit surface area as shown in Fig. 6. Then, the tendency in the variations of Q_{st} of Fig. 5 is correlated well with the variations of CO_2 working capacity of Fig. 6, which was clearly presented in Fig. S3 of SI. Specifically, *csq*-MOFs and *scu*-MOFs with medium pore sizes (P4P-MOFs) exhibit higher CO_2 working capacity than those with small pore sizes (P4T-MOFs) except several frameworks functionalized by multiple amine groups (*e.g.* BBB-MOFs), and both P4P-MOFs and P4T-MOFs possess higher working capacity than P4PP-MOFs with the largest pore size (Fig. 6a and c). In addition, we also noted that the tendency in the CO_2/N_2 selectivity of *csq*-MOFs and *scu*-MOFs is different from their CO_2 working capacity as shown in Fig. S3. By subtracting the Q_{st} of N_2 from that of CO_2, we found that the CO_2/N_2 selectivity depends on the Q_{st} difference between CO_2 and N_2 as demonstrated in Fig. S4, which accounts for the distinct tendencies observed in the CO_2 working capacity (Fig. 6) and CO_2/N_2 selectivity (Fig. 3b).

Regarding P4T-MOFs and P4P-MOFs in *csq* and *scu* topology, we compared the chemical structures of P4T and P4P. We found that the surface area of P4P with four additional aromatic rings is larger than P4T, probably leading to stronger MOF-adsorbate interactions in P4P-MOFs due to the enhanced quadrupole-dipole interaction that exceeds the pore confinement effects caused by the overlapped potential wells in small P4T-MOFs. Thereby, we further computed the MOF-CO_2 and CO_2-CO_2 interaction energy through averaging the total host-adsorbate and adsorbate-adsorbate interaction energy by the total number of adsorbate molecules (Fig. S6). The results demonstrate that MOF-CO_2 interaction dominates the

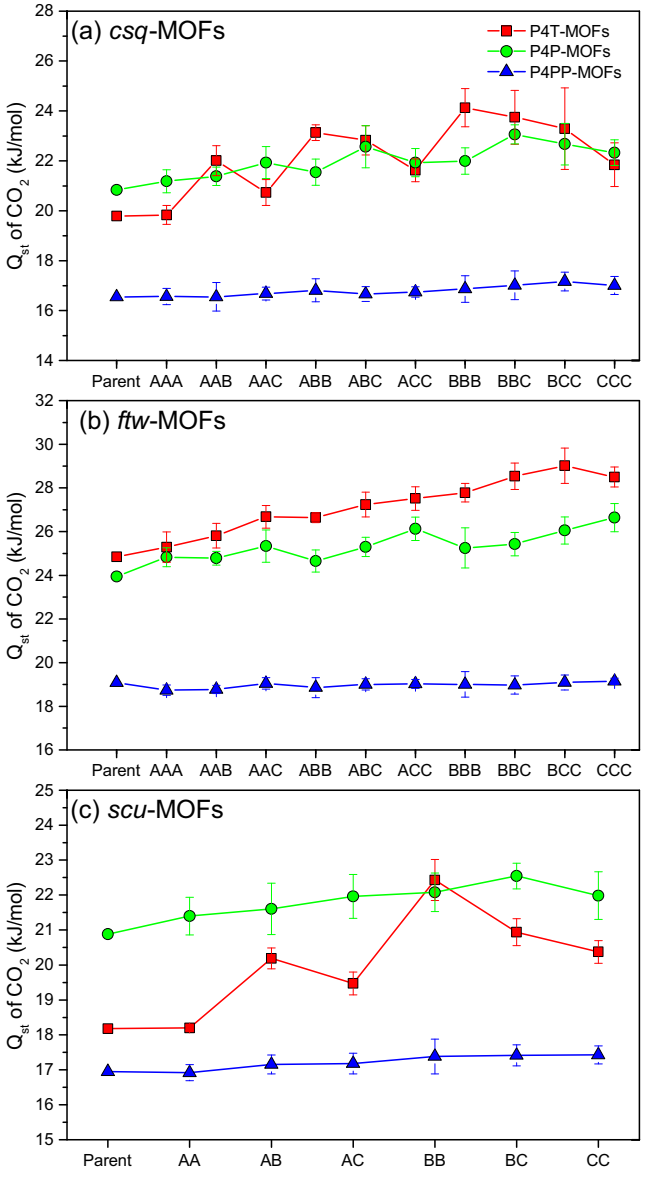

Fig. 5. The heat of desorption (Q_{st}) of CO_2 at 298 K and 1 bar. (a) Q_{st} of CO_2 in *csq*-MOFs, (b) Q_{st} of CO_2 in *ftw*-MOFs, (c) Q_{st} of CO_2 in *scu*-MOFs.

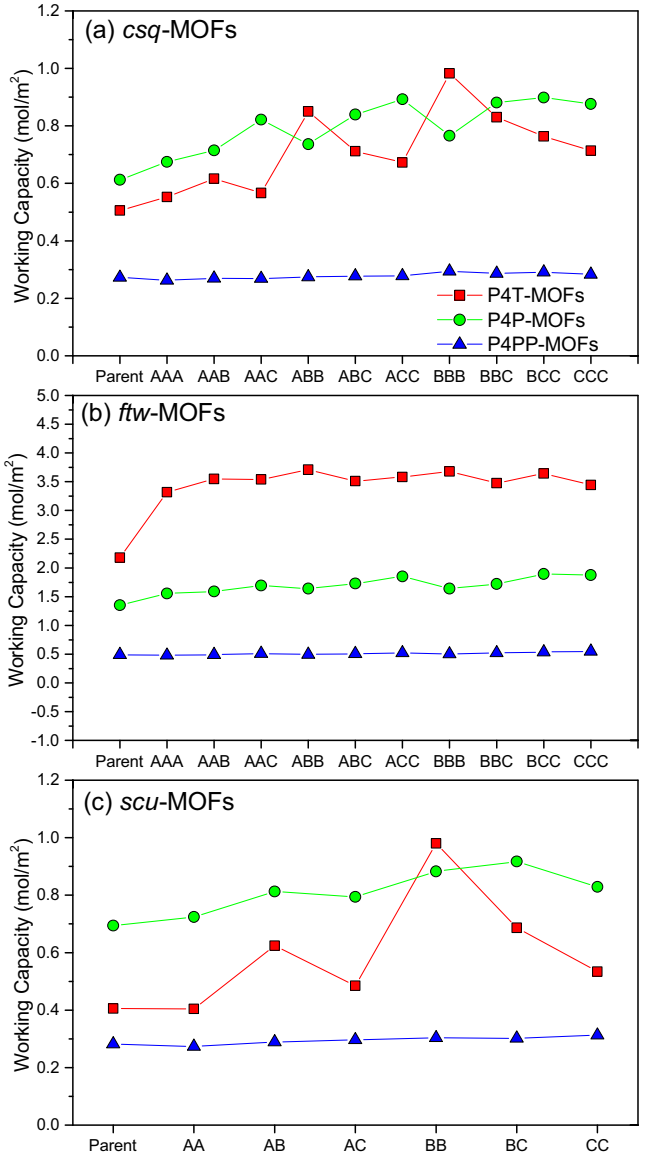

Fig. 6. The CO_2 working capacity of (a) *csq*-,(b) *ftw*-, (c) *scu*-MOFs at 298 K The red, green and blue symbols represent P4T-MOFs, P4P-MOFs and P4PP-MOFs, respectively. (For interpretation of the references to colour in this figure legend, the reader is referred to the web version of this article.)

CO_2 adsorption, and *ftw*-MOFs possess higher host-adsorbate interaction energy than *csq* and *scu* counterparts, in agreement with the observations in Fig. 6. Besides, the P4PP-MOFs with the largest pore sizes exhibited the lowest interaction strength compared with their counterparts consisting of P4P and P4T. In both *csq*-MOFs and *scu*-MOFs, parent P4P-MOFs with medium pore size exhibited higher framework-CO_2 interaction energy than parent P4T-MOFs, similar to their performance in CO_2 adsorption (Fig. 6). Similar tendency was also inspected in a majority of their functionalized derivatives except for certain structures with multiple amine groups that exhibited ultrahigh affinity towards CO_2, which will be discussed in detail later.

Although *ftw*-P4T-MOFs exhibit higher CO_2 working capacity than *ftw*-P4P-MOFs, the host-adsorbate interaction energy of *ftw*-P4T-MOFs is close to that of *ftw*-P4P-MOFs (Fig. 6b), which may be attributed to the different topological impacts where the differing spatial organizations of building blocks including metal nodes and organic linkers result in varying geometrical properties. When comparing the pore size distributions of *ftw*-P4T-MOF and *ftw*-P4P-MOF (Fig. S7), the parent *ftw*-P4T-MOF possesses a large fraction of small pores (<5 Å) compared with *ftw*-P4P-MOF, and the short P4T without the additional four aromatic rings as in P4P, possesses more accessible adsorption sites towards CO_2 near metal clusters (Fig. 4d). Both a large amount of small pores and the increased adsorption sites will facilitate CO_2 uptake in *ftw*-P4T-MOFs. The promoted CO_2 adsorption in *ftw*-P4T-MOFs may depend on both the type of linkers as well as the pore size of frameworks, the vast majority of pores in *csq*-P4T-MOFs and *scu*-P4T-MOFs is larger (>5 Å) than the small pores in *ftw*-P4T-MOFs (Fig. S7), thus counterbalancing the improved adsorption resulting from the additional adsorption sites of P4T linkers.

On the other hand, the combination type of functional groups within frameworks imposes effects on CO_2 working capacity and CO_2/N_2 selectivity. Deng et al. (2010) reported that MTV-MOF-5 with three differing functionalized linkers exhibited enhanced CO_2 uptake in contrast to those with two differing functionalized linkers, similar to Chun et al.'s former study on $Zn_2(1,4\text{-bdc})_2$-(dabco) MOF (Chun et al., 2005). McDaniel et al. (2013) found that the synergistic enhancement in adsorption due to the interactions between adsorbates and functionalized linkers exhibited dependence on the MOF topology and the pore size (McDaniel et al., 2013). However, our study showed that mono-linker BBB-MOFs exhibit the highest CO_2 uptake and selectivity compared with three-linker ABC-MOFs (or two-linker AB-MOFs in *scu*) or two linker ABB-MOFs (or AB- and AC-MOFs in *scu*) as shown in Fig. 3, implicating the absence of synergistic effects in the CO_2 adsorption of the functionalized MOFs in this work. According to previous report, the MOFs with synergistic effects must contain interaction sites at which the adsorbates can interact simultaneously with multiple linkers or functional groups (McDaniel et al., 2013). Thus, the possibility for CO_2 adsorbates to simultaneously interact with multiple functional groups of *csq*-, *ftw*- and *scu*-MOFs of this work is low considering their big pore sizes and specific topology. Besides, instead of choosing the large and bulky functional groups as reported in MOF-5 by McDaniel et al. (2013), we adopted three functional groups (—F, —NH_2 and —OCH_3) with relatively small sizes compared with their pore sizes in this work, which is also unfavorable for synergistic effects. Moreover, the impact of functionalization type on CO_2 adsorption is not noticeable in MOFs with large pore sizes (*e.g.* P4PP-MOFs in Fig. 6), whose CO_2 working capacity and CO_2/N_2 selectivity are almost constant with the variation in the combination types of multiple functional groups in frameworks. With the decrease in the pore size, the dependence of CO_2 working capacity and selectivity on the combination type of functional groups becomes identifiable, especially for P4T-MOFs in *csq* and *scu* topology, which can be attributed to the enhanced host-adsorbate interactions upon functionalization (Fig. S6). On the contrary, the combination type of functional groups does not impose obvious effects on CO_2 adsorption performance of *ftw*-P4T-MOFs as well as their host-adsorbate interaction energy.

3.3. Interaction energy

In order to further explore the correlation between the combination type of functional groups and CO_2 adsorption performance, we separated the host-adsorbate interaction energy into two parts: Coulombic and van der Waals contributions as displayed in Fig. 7. Different from *csq*-P4T-MOFs and *scu*-P4T-MOFs, van der Waals potential dominates the host-adsorbate interaction of *ftw*-P4T-MOFs irrespective of the combination type of functional groups, which correlates with their similar CO_2 adsorption performance. Our previous study on *pcu*-MOFs (Li et al., 2017) has also revealed

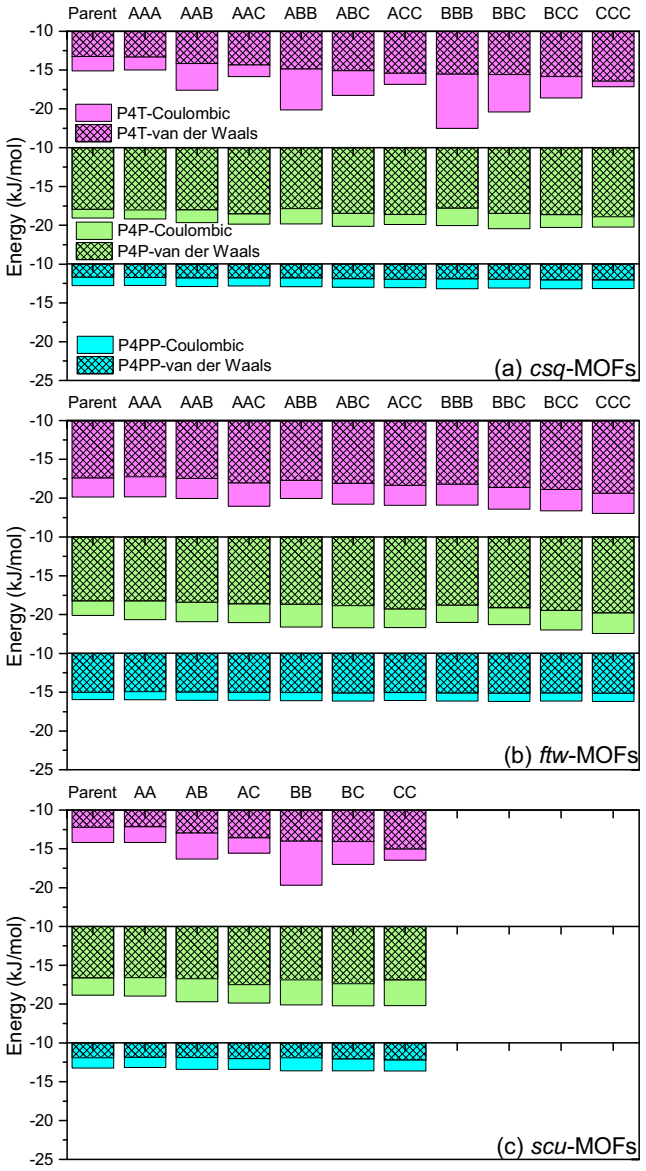

Fig. 7. The Coulombic and van der Waals contributions to the MOF host-adsorbate interaction energy of (a) *csq*-MOFs, (b) *ftw*-MOFs and (c) *scu*-MOFs calculated at 298 K and 1 bar from GCMC simulation. In order to clearly display the differences in the host-adsorbate interaction energy of various MOFs, the van der Waals interaction energy was shifted to −10 kJ/mol.

that the combination type of functional groups does not impose obvious impacts on the CO_2 adsorption performance of functionalized MOFs.

Furthermore, it was found that van der Waals potential played a dominant role in host-adsorbate interactions for most of the cases except for some amine-functionalized MOFs in *csq* and *scu*. The more amine groups were introduced into frameworks, the higher CO_2 working capacity and selectivity were obtained for *csq*-P4T-MOFs and *scu*-P4T-MOFs, which can be contributed by the significantly enhanced Coulombic interaction (Fig. 7), due to the relative large partial charges of —NH_2 as presented in Table S2. In additional, the Coulombic contribution of functionalized *csq*-P4T- and *scu*-P4T-MOFs was linearly decreased with the reduced content of amines in frameworks (*e.g.* BBB-P4T-MOFs, BBC-P4T-MOFs, BCC-P4T-MOFs and CCC-P4T-MOFs in *csq*) as demonstrated in Fig. S8. From another point of view, among —F, —NH_2 and —OCH_3, Lewis basic —NH_2 exhibits strong interaction with Lewis acid CO_2 as reported in previous study (Choi et al., 2012), thus —NH_2 functionalization brings in the most significant enhancement in CO_2 adsorption. The free energy contours in Fig. 8 show that the amine-functionalized *csq*-P4T-MOFs (BBB) exhibits larger attraction region than those functionalized by —F and —OCH_3 groups, consistent with their higher CO_2 uptake. Similar result was observed in *scu*-P4T-MOFs of Fig. S9. Whereas no obvious discrepancy was noticed in functionalized *ftw*-P4T-MOFs of Fig. S10, which is in agreement with their host-adsorption interaction energy in Fig. 7b.

In order to clarify the differences among their free energies, we further computed the free energy distribution of P4T-MOFs as shown in Figs. S11 and S12. The results show that the free energy of *ftw*-MOFs is mostly distributed at more attractive region followed by *scu*- and *csq*-MOFs, similar to the trend in their CO_2 capture performance. It was also found that the minimum free energy of *csq*-, *ftw*- and *scu*-P4T-MOFs also exhibit similar tendency to their CO_2 adsorption performance (Table S3). In addition, amine-functionalized P4T-MOFs exhibited more attractive regions than those functionalized by —F or —OCH_3 as shown in Fig. S12, consistent with the trend in CO_2 uptake. On the contrary, in large pore-sized frameworks, functionalities contributed slightly to the host-adsorbate interaction, thus leading to nearly identical van der Waals and Columbic interaction potentials in diversely functionalized P4PP-MOFs in Fig. 7, which is consistent with their CO_2 adsorption performance shown in Fig. 6.

3.4. Enhanced adsorption performance

For clear comparison of the enhanced adsorption performance of all MOFs, Fig. 9 summarizes the enhanced percentage in CO_2 working capacity and CO_2/N_2 selectivity of the functionalized *csq*-, *ftw*- and *scu*-MOFs in contrast to their parent counterparts, where pore-size dependence was obviously inspected, *i.e.* the enhancement in both CO_2 uptake and CO_2/N_2 selectivity decreases with the increase in the linker length or pore sizes of frameworks. P4PP-MOFs in *csq*, *ftw* and *scu* presented the similarly lowest enhancement. On average, *ftw*-P4T-MOFs exhibit the highest enhancement percentage than their counterparts. Whereas amine-functionalized BBB-P4T-MOF in *scu* exhibited the highest enhancement in CO_2 working capacity and selectivity, followed by BBB-P4T-MOF in *csq* and *ftw*, indicating that the CO_2 adsorption performance was obviously affected by the framework topology. Introducing functional groups that interact strongly with adsorbates into small sized frameworks in proper topology will give rise to the highest enhancement in their adsorption performance in contrast to pristine MOFs.

Functionalization cannot always enhance CO_2 uptake and CO_2/N_2 selectivity of MOFs, especially in MOFs with large pore sizes. Thereby, no evident increase in the CO_2 working capacity and selectivity of functionalized P4PP-MOFs compared to their parent counterparts was observed in Fig. 9. When modified by —F groups ("A") in various topologies, especially for *ftw*-P4PP-MOFs, their CO_2 adsorption capacity and selectivity were even slightly reduced. According to Torrisi et al.'s report, halogen substituents are unlikely to substantially enhance CO_2 affinity towards MOFs due to their electron-withdrawing effect on the aromatic ring of linkers, which destabilizes the CO_2 adsorption interaction (Torrisi et al., 2009). Nevertheless, when the pore size of frameworks is sufficiently small, halogen substitution is able to facilitate the CO_2 adsorption performance in MOFs due to the confinement effects

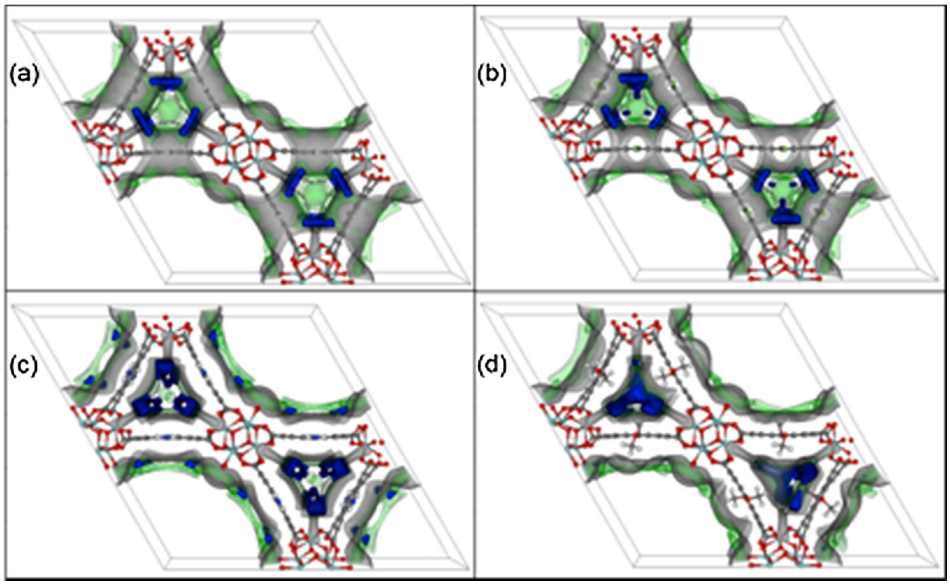

Fig. 8. Free energy contours of *csq*-P4T-MOFs, the gray regions represent the MOF surface with the free energy of +25 kJ/mol, the green regions represent the CO_2 adsorption sites with the free energy of −10 kJ/mol and the blue ones represent the adsorption site with the free energy of −15 kJ/mol for (a) parent *csq*-P4T-MOFs, (b) AAA-*csq*-P4T-MOFs, (c) BBB-*csq*-P4T- MOFs and (d) CCC-*csq*-P4T- MOFs. (For interpretation of the references to colour in this figure legend, the reader is referred to the web version of this article.)

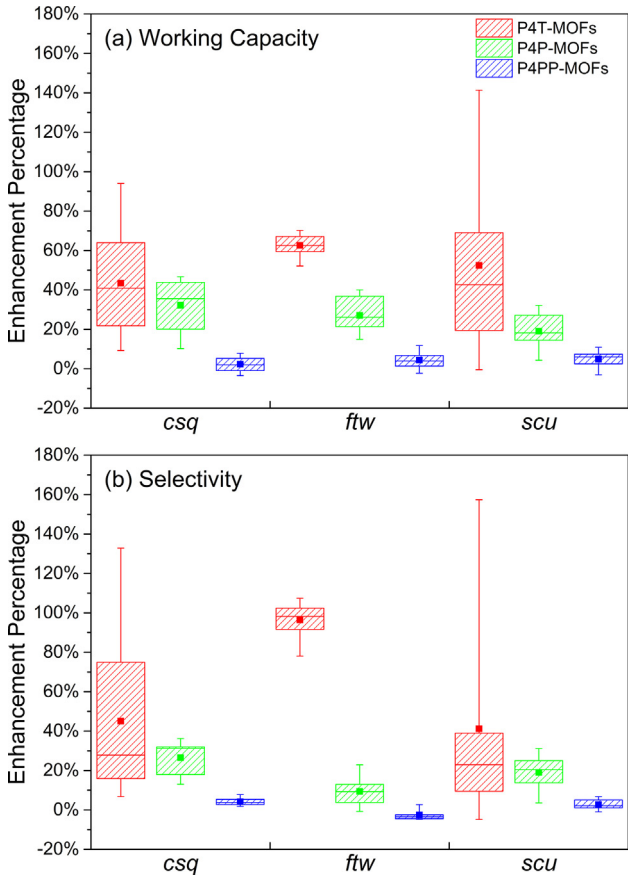

Fig. 9. The enhanced percentage in (a) CO_2 working capacity and (b) CO_2/N_2 selectivity of functionalized MOFs in contrast to their parent counterparts. The red, green and blue symbols represent P4T-MOFs, P4P-MOFs, and P4PP-MOFs, respectively. The horizontal line in the rectangular box denotes the median value of the group, and the small solid square represents the mean value of the derived MOFs of the same family. The lower and upper boundaries of the rectangular box represent the lower (first quartile or Q1) and upper (third quartile or Q3) hinge, respectively. The lower and upper bars represent the lower (minimum, which is calculated as Q1 − 1.5 × the interquartile range (IQR) that spans the first quartile to the third quartile range (IQR = Q3-Q1)) and upper (maximum, which is calculated as Q3 + 1.5 × IQR) fence, respectively. The points above or below the upper and lower fence are considered outliers, which are more than three times IQR above the third quartile or below the first quartile. (For interpretation of the references to colour in this figure legend, the reader is referred to the web version of this article.)

(Wilmer et al., 2012; Zhang et al., 2013). This could explain the enhanced CO_2 uptake in —F functionalized P4T-MOFs and the decreased performance in P4PP-MOFs functionalized by —F groups (Fig. 6).

4. Conclusions

In order to explore the effects of the topology, the pore size and the functionality of MOFs on carbon capture performance, frameworks in *csq*, *ftw* or *scu* topologies composed of identical Zr-metal node and organic linkers, *i.e.* P4T, P4P and P4PP in varying lengths, respectively, were generated for unbiased comparison by GCMC simulations. Regarding the topology effects, MOFs constructed by identical building blocks but in different topologies exhibit dissimilar trends in the variations of their geometrical properties. In terms of the CO_2 adsorption performance, *ftw*-MOFs obtained from GCMC simulation exhibit the highest CO_2 working capacity and CO_2/N_2 selectivity followed by *scu*-MOFs and *csq*-MOFs, which is mainly resulted from the small pore sizes of *ftw*-MOFs. Interestingly, the CO_2 adsorption performance of *ftw*-MOFs increases with the decrease in pore sizes, similar to the tendency observed in MOFs of *pcu* topology in previous study (Li et al., 2017). Whereas *csq*-MOFs and *scu*-MOFs with medium pore sizes (P4P) display the highest adsorption performance followed by smallest P4T-MOFs and largest P4PP-MOFs. Such a trend is attributed to the enhanced MOF-CO_2 interaction energy of P4P-MOFs in *csq* and *scu* due to the strong dipole-quandrupole interaction compared with their P4T counterparts, which is not dominant in the CO_2 adsorption of *ftw*-P4P-MOFs.

The influence of functionalization was studied by modifying each organic ligand by —F, —NH_2 and —OCH_3 to generate mixed linker or mono-linker MOFs, respectively. The combination type of functional groups imposes significant impact on CO_2 adsorption performance as well, which varies depending on the topology and pore size. In general, the adsorption performance of *csq*-P4T-MOFs and *scu*-P4T-MOFs were most greatly improved upon functionalization, followed by P4P-MOFs and P4PP-MOFs, indicating the pore-size dependent improvement in CO_2 adsorption performance of MOFs, consistent with our previous study (Li et al., 2017). Among a variety of combination types of functional groups, *csq*-P4T-MOFs and *scu*-P4T-MOFs functionalized by multiple —NH_2 groups exhibit the highest CO_2 working capacity and CO_2/N_2 selectivity than their parent counterparts, which is mainly ascribed to the enhanced Coulombic interactions between CO_2 and —NH_2 groups. However, the performance of *ftw*-P4T-MOFs is slightly affected by the combination type of functional groups within frameworks, which is attributed to the prevailing role of host-adsorbate interaction contributed by organic linkers instead of functionalities in small pores (<5 Å).

In summary, by restricting the frameworks to the predefined topology (*csq*, *ftw* or *scu*) using the linkers of varying lengths (P4T, P4P and P4PP) as well as specific functional groups (—F, —NH_2, —OCH_3), this work provides useful insights into the impacts of the topology, the pore size and the functional group of frameworks on CO_2 capture performance of MOFs, which may help guide relevant experimental research of the community. Nevertheless, the pore-size dependence of adsorption performance is still challenging, which may be greatly affected by the type of linkers and the framework topology. Given the limited types of the topology, linkers and functional groups employed in this work, further extensive study in this field is required for fully understanding the effects of the topology, the pore size and the functionality on CO_2 capture performance of MOFs.

Acknowledgements

This work was supported by the National Natural Science Foundation of China (NSFC) under Project No. 51606081. S. L. thanks the support from Basic Research Foundation of Shenzhen under Contract No. JCYJ20160506170043770. The work was carried out at National Supercomputer Center in Shenzhen, and the calculations were performed on TianHe-1(A).

Appendix A. Supplementary material

Supplementary data associated with this article can be found, in the online version, at https://doi.org/10.1016/j.ces.2018.05.042.

References

Bae, Y.S., Snurr, R.Q., 2011. Development and evaluation of porous materials for carbon dioxide separation and capture. Angew. Chem. Int. Edit. 50, 11586–11596.

Bai, Y., Dou, Y.B., Xie, L.H., Rutledge, W., Li, J.R., Zhou, H.C., 2016. Zr-based metal-organic frameworks: design, synthesis, structure, and applications. Chem. Soc. Rev. 45, 2327–2367.

Banerjee, R., Furukawa, H., Britt, D., Knobler, C., O'Keeffe, M., Yaghi, O.M., 2009. Control of pore size and functionality in isoreticular zeolitic imidazolate

frameworks and their carbon dioxide selective capture properties. J. Am. Chem. Soc. 131, 3875–3877.
Britt, D., Furukawa, H., Wang, B., Glover, T.G., Yaghi, O.M., 2009. Highly efficient separation of carbon dioxide by a metal-organic framework replete with open metal sites. Proc. Natl. Acad. Sci. 106, 20637–20640.
Choi, S., Watanabe, T., Bae, T.-H., Sholl, D.S., Jones, C.W., 2012. Modification of the Mg/DOBDC MOF with amines to enhance CO_2 adsorption from ultradilute gases. J. Phys. Chem. Lett. 3, 1136–1141.
Chun, H., Dybtsev, D.N., Kim, H., Kim, K., 2005. Synthesis, X-ray crystal structures, and gas sorption properties of pillared square grid nets based on paddle-wheel motifs: Implications for hydrogen storage in porous materials. Chem.-Eur. J. 11, 3521–3529.
Collins, S.P., Daff, T.D., Piotrkowski, S.S., Woo, T.K., 2016. Materials design by evolutionary optimization of functional groups in metal-organic frameworks. Sci. Adv. 2, e1600954.
Couck, S., Denayer, J.F.M., Baron, G.V., Remy, T., Gascon, J., Kapteijn, F., 2009. An amine-functionalized MIL-53 metal-organic framework with large separation power for CO_2 and CH_4. J. Am. Chem. Soc. 131, 6326–6327.
D'Alessandro, D.M., Smit, B., Long, J.R., 2010. Carbon dioxide capture: prospects for new materials. Angew. Chem. Int. Edit. 49, 6058–6082.
Deng, H.X., Doonan, C.J., Furukawa, H., Ferreira, R.B., Towne, J., Knobler, C.B., Wang, B., Yaghi, O.M., 2010. Multiple functional groups of varying ratios in metal-organic frameworks. Science 327, 846–850.
Devic, T., Horcajada, P., Serre, C., Salles, F., Maurin, G., Moulin, B., Heurtaux, D., Clet, G., Vimont, A., Greneche, J.M., Le Ouay, B., Moreau, F., Magnier, E., Filinchuk, Y., Marrot, J., Lavalley, J.C., Daturi, M., Ferey, G., 2010. Functionalization in flexible porous solids: effects on the pore opening and the host-guest interactions. J. Am. Chem. Soc. 132, 1127–1136.
Dubbeldam, D., Calero, S., Ellis, D.E., Snurr, R.Q., 2014. RASPA, version 1.9. Northwestern University, Evanston, IL.
Eddaoudi, M., Kim, J., Rosi, N., Vodak, D., Wachter, J., O'Keeffe, M., Yaghi, O.M., 2002. Systematic design of pore size and functionality in isoreticular MOFs and their application in methane storage. Science 295, 469–472.
Essmann, U., Perera, L., Berkowitz, M.L., Darden, T., Lee, H., Pedersen, L.G., 1995. A smooth particle mesh Ewald method. J. Chem. Phys. 103, 8577–8593.
Evans, J.D., Sumby, C.J., Doonan, C.J., 2014. Post-synthetic metalation of metal-organic frameworks. Chem. Soc. Rev. 43, 5933–5951.
Farha, O.K., Yazaydin, A.O., Eryazici, I., Malliakas, C.D., Hauser, B.G., Kanatzidis, M.G., Nguyen, S.T., Snurr, R.Q., Hupp, J.T., 2010. De novo synthesis of a metal-organic framework material featuring ultrahigh surface area and gas storage capacities. Nat. Chem. 2, 944–948.
Furukawa, H., Cordova, K.E., O'Keeffe, M., Yaghi, O.M., 2013. The chemistry and applications of metal-organic frameworks. Science 341, 1230444.
Hafner, J., 2008. Ab-initio simulations of materials using VASP: Density-functional theory and beyond. J. Comput. Chem. 29, 2044–2078.
Jiang, H.L., Feng, D.W., Liu, T.F., Li, J.R., Zhou, H.C., 2012. Pore surface engineering with controlled loadings of functional groups via click chemistry in highly stable metal-organic frameworks. J. Am. Chem. Soc. 134, 14690–14693.
Kong, X., Deng, H., Yan, F., Kim, J., Swisher, J.A., Smit, B., Yaghi, O.M., Reimer, J.A., 2013. Mapping of functional groups in metal-organic frameworks. Science 341, 882–885.
Li, J.R., Sculley, J., Zhou, H.C., 2012. Metal-organic frameworks for separations. Chem. Rev. 112, 869–932.
Li, S., Chung, Y.G., Simon, C.M., Snurr, R.Q., 2017. High-throughput computational screening of multivariate metal-organic frameworks (MTV-MOFs) for CO_2 capture. J. Phys. Chem. Lett. 8, 6135–6141.
Liu, D., Zhong, C., 2010. Understanding gas separation in metal-organic frameworks using computer modeling. J, Mater, Chem. 20, 10308–10318.
Liu, J., Thallapally, P.K., McGrail, B.P., Brown, D.R., Liu, J., 2012. Progress in adsorption-based CO_2 capture by metal-organic frameworks. Chem. Soc. Rev. 41, 2308–2322.
Long, J.R., Yaghi, O.M., 2009. The pervasive chemistry of metal-organic frameworks. Chem. Soc. Rev 38, 1213–1214.
Manz, T.A., Limas, N.G., 2016. Introducing DDEC6 atomic population analysis: part 1. Charge partitioning theory and methodology. RSC Adv. 6, 47771–47801.
McDaniel, J.G., Yu, K., Schmidt, J.R., 2013. Microscopic origins of enhanced gas adsorption and selectivity in mixed-linker metal-organic frameworks. J. Phys. Chem. C 117, 17131–17142.
McDonald, T.M., Mason, J.A., Kong, X.Q., Bloch, E.D., Gygi, D., Dani, A., Crocella, V., Giordanino, F., Odoh, S.O., Drisdell, W.S., Vlaisavljevich, B., Dzubak, A.L., Poloni, R., Schnell, S.K., Planas, N., Lee, K., Pascal, T., Wan, L.W.F., Prendergast, D., Neaton, J.B., Smit, B., Kortright, J.B., Gagliardi, L., Bordiga, S., Reimer, J.A., Long, J. R., 2015. Cooperative insertion of CO_2 in diamine-appended metal-organic frameworks. Nature 519, 303–308.
Potoff, J.J., Siepmann, J.I., 2001. Vapor-liquid equilibria of mixtures containing alkanes, carbon dioxide, and nitrogen. AIChE J. 47, 1676–1682.
Rappe, A.K., Casewit, C.J., Colwell, K.S., Goddard, W.A., Skiff, W.M., 1992. UFF, a full periodic table force field for molecular mechanics and molecular dynamics simulations. J. Am. Chem. Soc. 114, 10024–10035.
Reinsch, H., van der Veen, M.A., Gil, B., Marszalek, B., Verbiest, T., de Vos, D., Stock, N., 2013. Structures, sorption characteristics, and nonlinear optical properties of a new series of highly stable aluminum MOFs. Chem. Mater. 25, 17–26.
Segall, M., et al., 2002. Materials studio CASTEP, version 2.2. Accelrys: San Diego CA.
Sekizkardes, A.K., Islamoglu, T., Kahveci, Z., El-Kaderi, H.M., 2014. Application of pyrene-derived benzimidazole-linked polymers to CO_2 separation under pressure and vacuum swing adsorption settings. J. Mater. Chem. A 2, 12492–12500.
Sim, J., Yim, H., Ko, N., Choi, S.B., Oh, Y., Park, H.J., Park, S., Kim, J., 2014. Gas adsorption properties of highly porous metal-organic frameworks containing functionalized naphthalene dicarboxylate linkers. Dalton Trans. 43, 18017–18024.
Sumida, K., Rogow, D.L., Mason, J.A., McDonald, T.M., Bloch, E.D., Herm, Z.R., Bae, T.-H., Long, J.R., 2012. Carbon dioxide capture in metal-organic frameworks. Chem. Rev. 112, 724–781.
Tanabe, K.K., Cohen, S.M., 2011. Postsynthetic modification of metal-organic frameworks-a progress report. Chem. Soc. Rev. 40, 498–519.
Torrisi, A., Mellot-Draznieks, C., Bell, R.G., 2009. Impact of ligands on CO_2 adsorption in metal-organic frameworks: first principles study of the interaction of CO_2 with functionalized benzenes. I. Inductive effects on the aromatic ring. J. Chem. Phys. 130, 194703.
Willems, T.F., Rycroft, C., Kazi, M., Meza, J.C., Haranczyk, M., 2012. Algorithms and tools for high-throughput geometry-based analysis of crystalline porous materials. Micropor. Mesopor. Mater. 149, 134–141.
Wilmer, C.E., Farha, O.K., Bae, Y.-S., Hupp, J.T., Snurr, R.Q., 2012. Structure-property relationships of porous materials for carbon dioxide separation and capture. Energy Environ. Sci. 5, 9849–9856.
Yuan, S., Chen, Y.-P., Qin, J.-S., Lu, W., Zou, L., Zhang, Q., Wang, X., Sun, X., Zhou, H.-C., 2016. Linker installation: engineering pore environment with precisely placed functionalities in zirconium MOFs. J. Am. Chem. Soc. 138, 8912–8919.
Yuan, S., Lu, W., Chen, Y.-P., Zhang, Q., Liu, T.-F., Feng, D., Wang, X., Qin, J., Zhou, H.-C., 2015. Sequential linker installation: precise placement of functional groups in multivariate metal-organic frameworks. J. Am. Chem. Soc. 137, 3177–3180.
Zhang, D.-S., Chang, Z., Li, Y.-F., Jiang, Z.-Y., Xuan, Z.-H., Zhang, Y.-H., Li, J.-R., Chen, Q., Hu, T.-L., Bu, X.-H., 2013. Fluorous metal-organic frameworks with enhanced stability and high H_2/CO_2 storage capacities. Sci. Rep. 3, 3312.